Changes in morphology and optical properties of sclera and choroidal layers due to hyperosmotic agent

Raiyan T. Zaman
Narasimhan Rajaram
Brandon S. Nichols
Henry G. Rylander III
Tianyi Wang
James W. Tunnell
Ashley J. Welch

Changes in morphology and optical properties of sclera and choroidal layers due to hyperosmotic agent

Raiyan T. Zaman,a Narasimhan Rajaram,b Brandon S. Nichols,a Henry G. Rylander III,a Tianyi Wang,a James W. Tunnell,a and Ashley J. Welcha

aThe University of Texas at Austin, Department of Biomedical Engineering, 1 University Station C0800, Austin, Texas 78712-0238
bDuke University, Department of Biomedical Engineering, 136 Hudson Hall, P.O. Box 90281, Durham, North Carolina 27708

Abstract. Light scattering in the normally white sclera prevents diagnostic imaging or delivery of a focused laser beam to a target in the underlying choroid layer. In this study, we examine optical clearing of the sclera and changes in blood flow resulting from the application of glycerol to the sclera of rabbits. Recovery dynamics are monitored after the application of saline. The speed of clearing for injection delivery is compared to the direct application of glycerol through an incision in the conjunctiva. Although, the same volume of glycerol was applied, the sclera cleared much faster (5 to 10 s) with the topical application of glycerol compared to the injection method (3 min). In addition, the direct topical application of glycerol spreads over a larger area in the sclera than the latter method. A diffuse optical spectroscopy system provided spectral analysis of the remitted light every two minutes during clearing and rehydration. Comparison of measurements to those obtained from phantoms with various absorption and scattering properties provided estimates of the absorption coefficient and reduced scattering coefficient of rabbit eye tissue. © 2011 Society of Photo-Optical Instrumentation Engineers (SPIE). [DOI: 10.1117/1.3599985]

Keywords: hyperosmotic agents; optical clearing; optical properties; reduced scattering coefficient; absorption coefficient; diffuse optical spectroscopy; linear-probe; sclera.

Paper 09199PRRRRRR received May 17, 2009; revised manuscript received May 13, 2011; accepted for publication May 23, 2011; published online Jul. 13, 2011.

1 Introduction

Light scattering in the normally white sclera prevents diagnostic imaging or delivery of a focused laser beam to targets in the underlying choroidal layer. Methods to optically clear the sclera include localized pressure to decrease local water fraction and delivery of a hyperosmotic agent that dehydrates and provides index matching of collagen fibers.

Hyperosmotic agents such as 100% anhydrous glycerol, substantially increase the penetration depth of light in sclera[1–10] by reducing light scattering.[11–13] Optical clearing provides a low attenuation path for therapeutic laser applications and prevents excessive damage to sclera.[14] However, glycerol causes a decrease in blood flow when this agent is used in skin.[15] Thus, these experiments are designed to examine the dynamics of blood volume fraction and mean blood vessel diameter in the conjunctiva and choroid after the application of glycerol using diffuse optical spectroscopy (DOS) measurements.

A number of researchers have demonstrated the ability of diffuse optical spectroscopy to noninvasively monitor optical properties and hence physiology of tissue. Light is delivered and collected with an optical fiber probe that is placed in contact with the tissue surface. Weak light pulses sample the tissue beneath the probe without causing damage and provide valuable information regarding the scattering and absorption properties of tissue. The scattering from tissue can be correlated to tissue micro-architecture and is due to cells in the epithelial layer and collagen in the stroma. Tissue absorption is primarily caused by hemoglobin confined to blood vessels and melanin primarily in the choroid. Diffuse reflectance spectra are analyzed to determine blood volume fraction, blood oxygen saturation, blood vessel diameter, melanin concentration, and scattering. The development and validation of the DOS model has been described in detail earlier by Rajaram et al.[16] Analysis of the remitted light assumes a negative power law dependence of scattering with respect to wavelength.[17] Because hemoglobin is not homogeneously distributed in tissue, Beer's law does not suitably describe blood absorption for estimating hemoglobin concentration. The algorithm best suited to account for the inhomogeneous distribution of hemoglobin (contained in blood vessels) assumes confined distributions of absorbers; this model has been validated using tissue phantoms and Monte Carlo simulations.[18–20] By fitting the collected diffuse reflectance with a set of equations, oxygen saturation, mean vessel diameter, blood volume fraction, and scatter density can be estimated. Blood volume fraction and mean vessel diameter refer to total amount of blood sampled by the probe and the area to which it is confined, respectively. A brief description of DOS and the equations used to spectrally constrain the absorption and scattering are described in Secs. 2.8 and 2.9.

Previous optical clearing studies in skin have documented a decrease in blood flow and even closure of blood vessels,[15, 21] followed by vessel recovery as the concentration of hyperosmotic agent dissipates. These studies have proposed that dehydration and hydration of the hamster dorsal skin by

---

Address all correspondence to: Raiyan Zaman, The University of Texas at Austin, Biomedical Engineering, 1 University Station C0800, BME 1.344, Austin, Texas 78712; Tel: 512-471-1379; E-mail: raiyan_zaman@yahoo.com.

the application of a hyperosmotic agent and 0.9% saline, respectively, are primarily responsible for reducing light scattering observed in optical clearing. In our study, we examine the relationship between optical properties such as reduced scattering coefficient, absorption coefficient, and the various morphological features of tissue—melanin concentration, blood volume fraction, oxygen saturation, and blood vessel diameter.

This study examines the dynamics of optical properties and the effect glycerol has on the local vascular system. By injecting glycerol through the conjunctiva and making time series measurements with DOS, it is possible to follow dynamic changes in optical properties and the vascular system of the choroid and conjunctiva. DOS measurements continuously monitor blood oxygen saturation, blood vessel size, blood volume fraction, and scattering changes caused by the infusion of glycerol and subsequent rehydration of the system. Glycerol induces large changes in tissue scattering that may exceed the bounds of validity of typical DOS algorithms; the possibility of errors must be considered. Two additional measurements are included in this study: 1. the rate of clearing of an injection method of glycerol delivery compared to direct application of glycerol through an incision in the conjunctiva, and 2. visualization of the choroid after application of glycerol.

2 Methodology

2.1 Animal Preparation

Experiments were conducted on female SPF Dutch Belted ($n = 8$) rabbits weighing 4 to 5 lbs at the Animal Resource Center according to protocols approved by the Animal Care Committee of The University of Texas at Austin (IACUC # 06060801). Prior to experiments, rabbits were anesthetized with Glycopyrrolate 0.02 mg/kg intramuscularly (IM) followed by 5 mg/kg Xylazine and 40 mg/kg Ketamine hydrochloride (Rompun-Ketaset) in the proportions: 60% of 20 mg/ml Rompun to 40% of 100 mg/ml Ketaset by volume. Anesthesia was maintained with isoflurane (1.5 to 3%) inhalant. Isoflurane was supplemented by acepromazine (0.25 to 1.0 mg/kg) administered intramuscularly as needed for individual rabbits demonstrating a high tolerance to isoflurane. One hour prior to termination of isoflurane, buprenorphine 0.01 to 0.05 mg/kg was administered IM for any pain or discomfort.

Rabbits were positioned in the ventral recumbent position. Oxygen saturation, pulse rate, heart rate, and respiration rate were monitored every 15 min throughout the study using a vet/ox G2 digital pulse oxymeter (Heska Corp., Loveland, Colorado). Measurements were made via a shaved area of the feet or the ear depending on the best contact for recording. The animal's body temperature was maintained with a warm water blanket. Anesthetic and monitoring procedures were performed by a skilled technician from the Animal Resource Center at the University of Texas at Austin.

2.2 Dehydration/Hydration Cycle

Glycerol and saline were used to create "dehydration" and "hydration" cycles, by altering the osmotic pressure at the surface of the sclera. Glycerol removed water (dehydration);

glycerol concentration was decreased by either flooding the sclera with saline or by natural diffusion away from the site (natural re-hydration). Dehydration alters collagenous spacing and reduces light scattering.[21] During the dehydration cycle, 100% anhydrous glycerol was applied to the sclera by injection through the conjunctiva or glycerol was deposited on top of the sclera through a conjunctival incision. A single volume of 0.1 ml glycerol was injected one time prior to spectroscopy measurements. The first measurement time 0^+ was within 15 s of the completion of the injection, which required two minutes. The morphological changes were captured using a slit lamp connected with an EOS Digital SLR Canon camera; measurements were recorded at two minute intervals up to 26 min during the dehydration cycle. Morphological and optical property changes reached a steady state after 18 min. Therefore, only the first 18 min of measurements are presented in Sec. 3. The dehydrated tissue was then hydrated by applying a 0.9% saline solution. Dehydration and hydration cycles were repeated four times for the same duration of time. Hydration cycle measurements reached steady state within 12 min.

2.3 In Vivo Eye Model

In this study, we are interested in three layers of the *in vivo* eye model: 1. bulbur conjunctiva, 2. sclera, and 3. choroid. The bulbar conjunctiva is a thin (54.7 ± 1.9 μm) clear outermost epithelial membrane that covers the sclera.[22–24] The naturally white sclera is just beneath the conjunctiva, which is opaque due to its normal level of hydration. Collagen accounts for 90% of the dry weight of all mammalian sclera. In addition, some fine blood vessel arcades exist on both surfaces of the conjunctiva and sclera; however, sclera is mostly avascular and is anatomically similar to brain dura mater. The thickness of the sclera varies from 1000 μm at the posterior pole to 300 μm just behind the rectus muscle insertions. Sclera is continuous with the dura mater and the cornea, and provides an attachment for the extra ocular muscles. The choroid lies between the sclera and retinal pigment epithelium (RPE) and consists of four layers: 1. Haller's layer (outermost layer), 2. Sattler's layer, 3. Choriocapillaris, and 4. Bruch's membrane (innermost layer). Haller's and Sattler's layers consist of large and medium diameter blood vessels, respectively; Choriocapillaris layer has capillaries.[25] Melanin, a darkly-colored chromophore synthesized by melanocytes, occurs throughout the choroidal layer; absorption of light by melanin prevents uncontrolled reflections within the eye and increases vision.[26] The RPE is the pigmented cell layer just outside the neuro-sensory retina and is firmly attached to the underlying choroid.

The optical model illustrated in Fig. 1(a) depicts the light interaction with the three layers of eye tissue. We assume three different cases: 1. at baseline (before 100% anhydrous glycerol application), light entering the sclera undergoes multiple scattering events; 2. after glycerol application, light penetration depth increases allowing collimated and forward scattered light to reach the choroidal layer, and 3. as the sclera rehydrates, the sclera becomes less transparent, which increases backscattering. Figures 1(b)–1(d) illustrate these hypothesized scenarios.
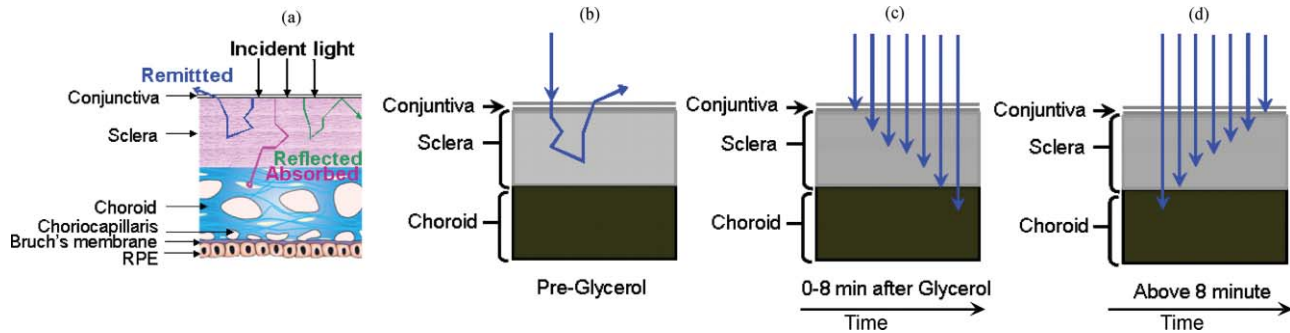
Fig. 1 Morphological and optical property change of the eye associated with optical clearing: (a) anatomy and light propagation in eye model, (b)–(d) light propagation in normal (baseline), dehydrated, and rehydrated tissue.

2.4 Surgical Procedure

A wire eye speculum was placed in the eye to retract the eyelids. The position of the eye was stabilized with a suture placed at the limbus. The suture helped to position the eye and provided access to the sclera for delivering the hyperosmotic agent. Injection sites were at least 5.0 mm from the limbus. We introduced glycerol close to the limbus area where the sclera was the thinnest (about 300 μm). Glycerol was delivered to sclera in two methods: injecting through bulbar conjunctiva (using a 27G 1/2 hypodermic needle from Beckton Dickinson, New Jersey) and direct topical application after making a 0.3 cm incision in the conjunctiva. The glycerol was injected very slowly due to its high viscosity. The glycerol was poured from the original container into a smaller airtight screw cap bottle for each experiment to prevent the glycerol from absorbing any moisture from the air due to its hygroscopic nature. Glycerol remaining after an experiment was discarded to prevent contamination.

2.5 Photography of Sclera Treated with Glycerol and Saline

An EOS digital SLR Canon camera (Digital Rebel XT, Japan) attached to a slit lamp (Topcon SL-6E) captured the morphological changes of the sclera and choroidal layers during the dehydration and hydration cycles. The camera shutter was triggered by digital single-lens reflex software using a computer. A photograph was taken of the *in vivo* sclera at baseline (pre-glycerol application), immediately after glycerol application (0^+ min), every two minutes up to 26 min, and after hydrating the sclera with 0.9% saline.

2.6 Diffuse Optical Spectroscopy System

The system used to collect the diffuse reflectance has been described in detail by Zaman et al.[27] Briefly, the DOS system consists of three main components: 1. a tungsten halogen lamp that produces a white light source (LS-1, Ocean Optics), 2. a custom-designed fiber-optic probe (core diameter = 200 μm; NA = 0.22; FiberTech Optica), and 3. a spectrometer (USB4000, Ocean Optics) (Fig. 2). The fiber-optic probe consists of two individual fibers, separated by 370 μm, that are terminated with SMA connectors. The source and detector fibers were connected

to the lamp and spectrometer, respectively. The analysis model is unique to the probe geometry used in this study.

We measured the diffuse reflectance spectrum from tissue over a wavelength range of 425 to 700 nm that includes most of the Soret band. The fiber-optic probe was placed in contact with the surface of the bulbar conjunctiva, and the average reflectance spectra was computed from three measurements for white light spectra (Fig. 3: average of all eight rabbits) at each time point that was reflected from eye tissue. Each reflectance spectra was collected within 100 milliseconds. Reflectance spectra before and after the application of glycerol were collected from the same location. Another set of reflectance spectrum was collected immediately after hydrating (0^+ min) the sclera with 0.9% saline and every two minutes up to 12 min. Prior to spectral analysis, recorded signals were corrected for system response by subtracting the detector dark current and normalizing the sample reflectance by the reflectance of a Lambertian reflector (Spectralon, Labsphere Inc.; 40% reflectance standard).

Analysis of data revealed that some results were affected by the time of day of the experiments: morning (AM) or afternoon (PM). Therefore, some results were grouped as AM or PM.

2.7 Sampling Depth Measurement

The sampling depth of optical fibers is a function of the source-detector separation distance and the optical properties of the tissue. Determination of the sampling depth assumes importance
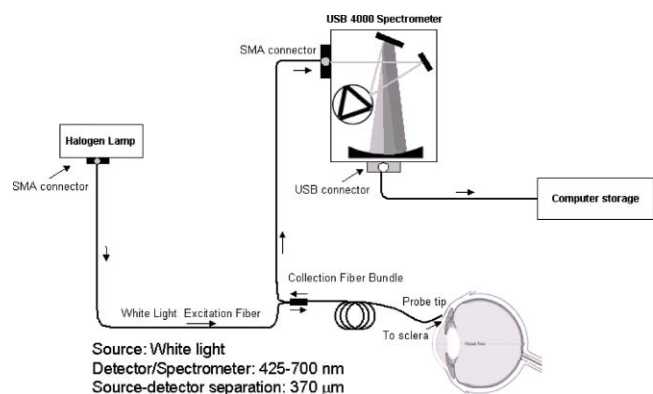
Fig. 2 Schematic illustration of the instrumentation setup for DOS system.
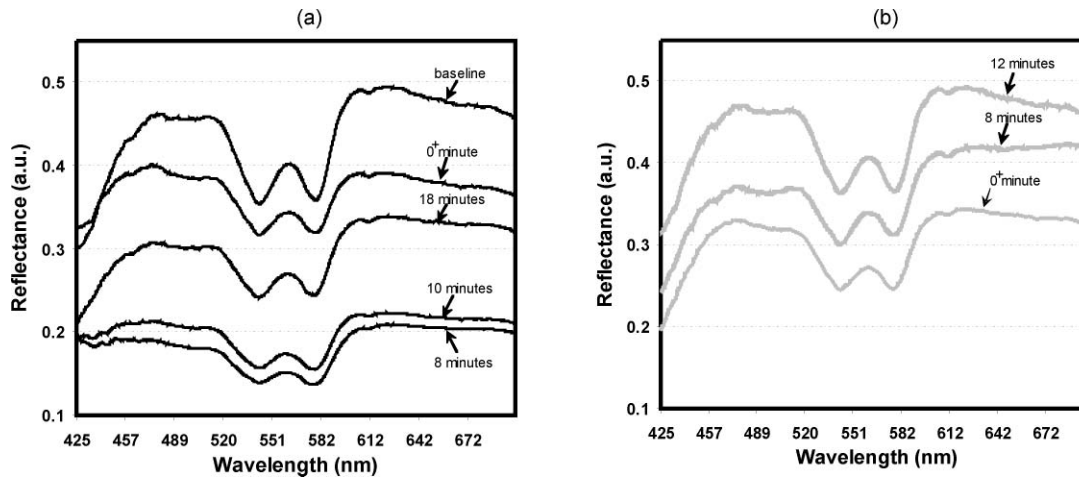
Fig. 3 Reflection spectrum of rabbit sclera measured using DOS system. (a) Dehydration cycle: plot of average reflection spectrum of sclera at baseline, 0^+, 8, 10, and 18 min post-clearing after glycerol injection. (b) Hydration cycle: plot of average reflection spectrum of sclera at 0^+, 8, 10, and 18 min after saline application. The mean spectrum was calculated from eight samples.

due to the multilayered nature of eye tissue. It is possible to approximate the reflected light as a volume average; however, as the hyperosmotic agent optically clears the sclera, it is important to know if the probe can sample reflectance from the choroid. Therefore, knowledge of the sampling depth is necessary.

Estimates of the changes in the sampling depth were obtained using a container (base painted with nonreflective black paint), which was filled with 10% diluted intralipid (10% intralipid:water with 1:9 ratio) solution to mimic the scattering of the natural sclera. The reduced scattering coefficient (μ_s') of the diluted intralipid solution at 630 nm was 1.0 to 5.0 mm^{-1}, which is somewhat lower than the physiological range of μ_s' for *in vitro* bovine and porcine sclera (3.58 to 10.09 mm^{-1}).[28] A LabVIEW interface (SD Instrument, MC2000 controller) controlled the position of the fiber optic probe of the DOS system. The fiber-optic probe was initially placed at the base of the phantom. The measured reflectance intensity was close to zero due to the nonreflective black paint. Subsequently, the probe was moved in the *z*-direction and the reflectance intensity was recorded at each 50-μm step. The experiment was continued until the reflectance intensity reached a constant value. The slope of the curve provided a measure of this particular probe's sampling depth. Based on our experiments, the average sampling depths were identified between 379 to 525 μm for the simulated white sclera. Table 1 illustrates various μ_s' values of the intralipid solutions and its associated sampling depth.

2.8 Tissue Phantoms—LUT-based Diffuse Optical Spectroscopy Inverse Model
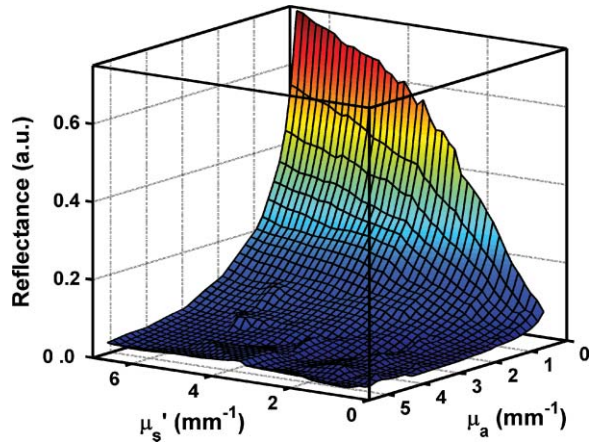
The diffusion approximation is a traditional method for determining optical properties from diffuse reflectance measurements as described by Farrell et al.[29] or a modified form according to Kienle et al.[30] However, a drawback of these models is their lack of accuracy at close source-detector separations (less than one mean free path) and low albedo [$\mu_s'/(\mu_s' + \mu_a) < 0.9$]. We used a lookup table (LUT)-based DOS inverse algorithm to determine the optical properties from the diffuse reflectance measurements.

Briefly, the DOS inverse model is a database of experimental measurements of calibration standards of known optical properties and is unique to the fiber geometry. The DOS inverse model is valid for probe geometries with close source-detector separations and in tissue with low albedo. The development and validation of the LUT-based DOS inverse model has been previously described in detail by Rajaram et al.[16] Recently, the LUT model was validated for extracting blood vessel diameter using micro-fluidic devices in a scattering medium (μ_s' of 1.0 mm^{-1} at 630 nm).[31] The LUT-based DOS inverse model estimates the absorption (μ_a) and reduced scattering (μ_s') coefficient over a wide range of absorption and scattering values with associated errors of ±11.6 and ±5.9%, respectively.

We constructed LUT using calibration standards of known optical properties. These calibration standards were made with polystyrene microspheres (diameter = 1.0 μm; Poly-sciences) and 10% India ink (Salis International) dissolved in water to

Table 1 Measured sampling depth for various μ_s' at 630 nm.

μ_s' of diluted intralipid solution (mm^{-1})	Sampling depth (μm)
1.0	532
1.5	511
2.0	487
2.5	466
3.0	441
3.5	418
4.0	398
4.5	385
5.0	379

Fig. 4 Resulting LUT-based DOS inverse model consists of known optical properties of tissue phantom made from polystyrene bead with various concentration of India ink (10% concentration). The spectral dependence of reflectance spectra (R) results from the wavelength-dependent optical properties of reduced scattering $\mu'_s(\lambda)$ and absorption $\mu_a(\lambda)$. By constraining the scattering and absorption coefficients, optical properties such as scatterer size and density, melanin concentration, blood volume fraction, oxygen saturation, and blood vessel diameter are extracted. These optical properties are extracted from a single reflectance spectrum at different observation time similar to Fig. 3 that depicted the average of all eight rabbits.

simulate scattering and absorption, respectively. The physical thickness of the tissue phantom was 3.0 mm. Optically, the tissue phantom was considered as semi-infinite for the wavelengths of interest. The optical properties of the polystyrene microspheres and India ink were calculated using Mie theory and a UV-Vis spectrophotometer, respectively.

The LUT matrix (6×10) was constructed using reflectance measurements from 60 tissue phantoms with varying scattering $[\mu'_s(\lambda) = 0.25$ to 4 mm$^{-1}]$ and absorption parameters $[\mu_a(\lambda) = 0$ to 6.41 mm$^{-1}]$ that encompassed the range of optical properties found in tissue previously reported by Welch et al.[32] These 60 phantoms covered the entire range of the LUT matrix. The LUT of reflectance as a function of $\mu'_s(\lambda)$ and $\mu_a(\lambda)$ is illustrated in Fig. 4. A single reflectance spectrum at different observation times similar to Fig. 3 (the average reflectance trend from all eight rabbits) from *in vivo* rabbit eye tissue was statistically compared to the LUT to estimate the optical properties of the sclera and choroidal layers during baseline, dehydration, and hydration cycles.

2.9 Data Analysis

The optical properties of the sclera and choroidal layers are extracted from spectrally resolved diffuse reflectance spectra (R) fit to the unique LUT-based DOS inverse model (Fig. 4). The spectral dependence of R results from the wavelength-dependent optical properties of $\mu'_s(\lambda)$ and $\mu_a(\lambda)$. By constraining the scattering and absorption coefficients, optical properties such as scatterer size and density, melanin concentration, blood volume fraction, oxygen saturation, and blood vessel diameter are extracted. These optical properties are extracted from a single reflectance spectrum at different observation times. A nonlinear optimizing routine (average fit time 5 to 10 s) statistically adjusts the spectrally resolved diffuse reflectance spectra to ex-

tract the optical properties. The reduced scattering coefficient is constrained to the form

$$\mu'_s(\lambda) = \mu'_s(\lambda_0).\left[\frac{\lambda}{\lambda_0}\right]^{-B} \quad [mm^{-1}], \quad (1)$$

where $\lambda_0 = 630$ nm. Mourant et al. have shown that a power law dependence on wavelength is an ideal approximation of scattering in bulk tissue.[17] Here, scattering magnitude and scatterer size are represented by $\mu'_s(\lambda_0)$ and B, respectively. We assume that absorption in the visible range is due to melanin, oxy- and deoxy-hemoglobin, and calculate the absorption coefficient as a linear combination of absorbers

$$\mu_a^{total}(\lambda) = \mu_a^{Hb}(\lambda) + \mu_a^{mel}(\lambda) \quad [mm^{-1}]. \quad (2)$$

The absorption coefficient of melanin is modeled as $\mu_a(\lambda) = [mel].\varepsilon_{mel}(\lambda)$, where $[mel]$ represents melanin concentration (mg/ml) and $\varepsilon_{mel}(\lambda)$, the wavelength-dependent extinction coefficient of melanin $[mm^{-1}/(mg/ml)]$.

A correction factor accounts for the inhomogeneous distribution of blood in tissue, as described by van Veen et al.[19] This correction factor modifies the absorption coefficient of hemoglobin to account for the confined distribution of hemoglobin in blood vessels. The absorption coefficient of hemoglobin and the correction factor are represented by the following equations:

$$\mu_a^{Hb}(\lambda) = C_{corr}.cHb.\mu_a(\lambda) \quad [mm^{-1}], \quad (3)$$

$$C_{corr} = \left[\frac{1 - \exp(-\mu_a(\lambda).d)}{\mu_a(\lambda).d}\right], \quad (4)$$

where cHb represents the blood volume fraction, $\mu_a(\lambda)$ is the absorption coefficient of whole blood assuming a hemoglobin concentration of 150 g/l, and d is the mean vessel diameter (mm). The absorption coefficient of blood is calculated as

$$\mu_a(\lambda) = \alpha.\mu_{aHbO_2}^{blood}(\lambda) + (1 - \alpha).\mu_{aHb}^{blood}(\lambda) \quad [mm^{-1}], \quad (5)$$

where α is the oxygen saturation of blood, $\mu_{aHbO_2}^{blood}(\lambda)$ and μ_{aHb}^{blood} respectively represent the absorption coefficients of fully oxygenated and fully deoxygenated blood. The extinction coefficients for oxy- and deoxy-hemoglobin have been previously documented in the literature of Prahl.[33] Based on the constraining equations described above, a Levenberg-Marquadt nonlinear optimization fits the diffuse reflectance spectra to the LUT-based DOS model. The fit parameters—$\mu'_s(\lambda_0)$, B, $[mel]$, cHb, d, and α are constrained to vary within a physiologically relevant ranges of 0.55 to 3.2 mm^{-1}, 0.9 to 1.2, 0.001 to 0.05 mg/ml, 0.3 to 4.5%, 10 to 120 μm, and 0 to 1, respectively.[16] All of these fit parameters are simultaneously calculated once the reflectance spectra is fit to the LUT.

2.10 Statistical Analysis: Quadratic Mixed Regression Model

We analyzed data using a quadratic mixed regression model[34] (QMRM) with observation nested with rabbit. Independent variables in all models included time and hydration status. In addition, time square was included to investigate a possible quadratic effect. Four separate QMRMs were run with the above independence for each dependent variable.
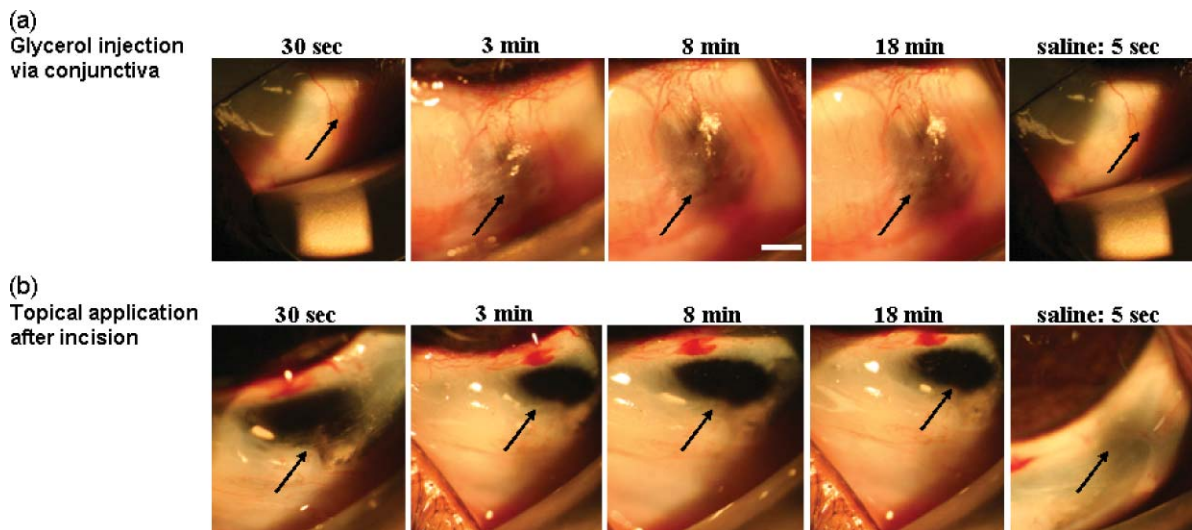
Fig. 5 Macroscopic time-lapsed images of rabbit eye model before, during, and after optical clearing. The time-lapse is indicated above each image as 0^+ (30 s), 3, 8, and 18 min post-clearing after glycerol injection (scale bar 0.5 cm).

3 Results

3.1 Sclera and Choroidal Layers: Change in Morphology

Photographs of the morphological changes in sclera and choroidal layers due to 100% anhydrous glycerol are shown in Fig. 5. Injection of glycerol through conjunctiva to the anterior surface of sclera shows initial significant clearing in three minutes, maximum transparency at eight minutes, and continued transparency for 10 to 15 min. Over the next 11 min the clear sclera became less transparent; when saline was injected, the sclera became completely opaque. Spectroscopic measurements were obtained when the injection method of glycerol was used to clear the sclera. Measurements were made during the clearing process and after the addition of saline at the 18-min mark. Direct topical application of glycerol after the incision of the conjunctiva caused the sclera to become transparent within 10 s, so time-resolved measurements of clearing with our instrumentation was not possible.

3.2 Diffuse Optical Spectroscopy

Baseline measurements prior to the injection of glycerol were expected to represent average optical properties of the conjunctiva and sclera because of limited penetration depth of the DOS light source in the white sclera. The low values of $\mu_a(\lambda)$ obtained from sclera at the baseline measurement [Figs. 7(c)–7(f)] confirm this hypothesis. Once the hyperosmotic agent was introduced, light penetration depth increased and reflection measurements were affected by the choroidal layer. All experimental conditions were kept constant throughout the experiment for each animal except for the starting time. Five rabbits were tested in the morning (AM) and three in the afternoon (PM) from 12:30 to 4:00. DOS data was separated post-hoc due to the observation of two different ranges of diameter for blood vessels. Therefore, optical property estimations were separated into two subgroups for $n = 5$ (AM) and $n = 3$ (PM) to identify any minor changes that may be the contributing factor of chronological changes in the rabbit eye.

3.2.1 Reduced scattering coefficient (μ'_s)

The μ'_s at 630 nm immediately decreased after glycerol injection as indicated by the 0^+ min value (30 s) in Figs. 6(a) and 6(b). The maximum reduction of 57% of the reduced scattering coefficient occurred at 10 min during the dehydration cycle for afternoon measurements (PM), and was followed by a gradual increase. After hydrating the tissue, reduced scattering coefficient increased linearly with respect to time and returned to baseline at 12 min after the application of saline. Afternoon (PM) baseline μ'_s was slightly but significantly higher than the morning (AM) measurements.

3.2.2 Absorption coefficient (μ_a)

Estimation of μ_a was based on 1. melanin concentration (mg/ml), 2. blood volume fraction (%), 3. oxygen (O_2) saturation (%), and 4. mean blood vessel diameter (μm). These values were extracted from the inverse solution of the measured reflectance over the wavelength band from 425 to 700 nm. Absorption as a function of wavelength prior to injection of glycerol (baseline) is shown in Fig. 7(a). Absorption coefficient spectrum in Fig. 7(a) showed a distinctive absorption peak between 525 to 600 nm wavelengths due to the presence of blood volume fraction in blood vessels at the bulbar conjunctiva, the site of glycerol injection as shown in Fig. 7(b). The variations of μ_a in sclera and choroidal layers during the dehydration and hydration cycles at 542 nm wavelength depicted a distinctive blood absorption peak with identifiable changes due to the hyperosmotic agent [Fig. 7(c)]. At a 650 nm wavelength, the variation of μ_a is not dominated by blood absorption [Fig. 7(d)]. The variation of μ_a, due to the dehydrated sclera and chorid, returned to baseline at 12 min after saline application to the eye.

Different patterns of the μ_a were noted in the AM and PM subgroups as shown in Figs. 7(e) and 7(f), respectively. Although, the maximum optical clearing occurred at eight minutes, the highest absorption peak at 650 nm wavelengths for the AM subgroup was observed at four minutes, unlike the PM
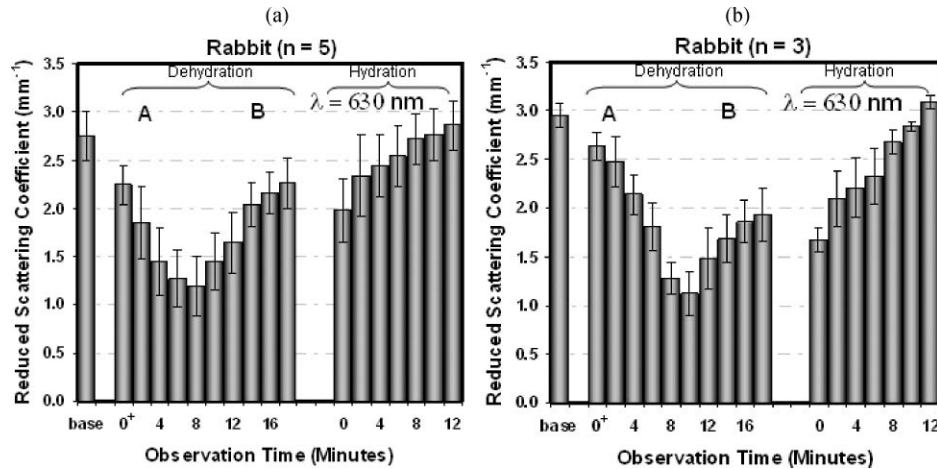
Fig. 6 μ_s' of rabbit eye sclera and choroid for (a) AM subgroup (morning measurement, $n = 5$) and (b) PM subgroup (afternoon measurement, $n = 3$) at baseline, after dehydration by injecting 100% anhydrous glycerol and hydration with 0.9% saline. Region A and B represent increase and decrease of optical clearing of sclera, respectively. All values are statistically significant ($p < 0.05$) for both the dehydration and hydration cycles (quadratic mixed regression model). Error bars in terms of standard deviation are computed based on the average of μ_s'.

subgroup. Also, the peak μ_a for the PM subgroup was slightly higher than the AM subgroup.

3.3 Melanin, Blood Volume Concentration, and Oxygen Saturation

Although, the conjunctiva and sclera layers did not contain many melanocytes, a trace amount of melanin concentration was indicated at baseline [Figs. 8(a) and 8(b)] due to the lower bound of melanin concentration in the diffusion inverse model. The lower bound was set to an extremely small nonzero number of 0.001 mg/ml for smooth execution of the model. When the sclera started to become optically clear during the dehydration cycle, the DOS system detected a high concentration of melanin from the choroidal layer. The maximum melanin concentration was detected at eight minutes, which corresponded to maximum clearing. Then, absorption gradually decreased as scattering increased in the sclera. The melanin concentration returned to its baseline measurement at 12 min after hydrating the tissue. The detected melanin concentration was slightly lower during the afternoon measurements for the three rabbits compared to the morning measurements. However, the difference between the morning and afternoon measurements was not statistically significant.

The initial baseline and the 0^+ min measurements of blood volume fraction represented the values from the anterior eye such as conjunctiva and part of the avascular sclera. The blood volume fraction is assumed to have a typical concentration of 150 g/l. The computed blood volume fraction in all eight rabbits increased $3.7\times$ at eight minutes during the dehydration cycle. The blood volume fraction for the afternoon measurement showed an initial decrease immediately after the application of glycerol. Most of the physiological absorption parameters, such as melanin concentration and blood volume fraction, returned to the baseline at the end of the hydration cycle.

At baseline, detected O_2 saturations for AM and PM subgroups were 82 and 86%, respectively [Figs. 8(e) and 8(f)]. Immediately after glycerol application at 0^+ min, the O_2 saturation increased up to 92 and 98%, respectively, during morning and

afternoon and decreased thereafter. During the dehydration cycle, the O_2 saturation reached minima (27 to 37%) at six minutes followed by a gradual increase. At the end of the dehydration cycle (18 min), the O_2 saturation reached its maximum saturation level of 99 to 100%. Variation in O_2 saturation between the morning and afternoon measurements was very different during the hydration cycle. The O_2 saturation for the AM subgroup gradually increased, unlike the PM subgroup where the saturation decreased first and then was followed by an increase. Both AM and PM subgroups showed an increase in O_2 saturation of 99 to 100% or hyperoxia at the end of the hydration cycle.

The diffusion inverse model computed a mean blood vessel diameter for each rabbit [Figs. 9(a) and 9(b)]. Thus, a total of eight mean blood vessel diameters data were collected at each observation point. After post-hoc analysis, these data fell into two subgroups: small and large microvasculatures. At baseline, the blood vessels diameter at the conjunctiva and scleral layers of the PM subgroup rabbit were smaller in size, 10 to 36 μm diameter, unlike the AM subgroup that were 91 to 120 μm. In addition to the physiological condition, the dynamics of the blood vessel diameter is not constant over time.[35] The small and large blood vessel groups for rabbits showed different dilation patterns upon glycerol application. The smaller blood vessels (PM) had a delayed increase in diameter during the dehydration cycle [Fig. 9(b)]. These vessels dilated to a maximum of $3.4\times$ or 64 ± 10 μm at 12 min. A slight decrease in diameter followed after 12 min without any outside hydration. After hydrating the sclera, an immediate enlargement of diameter was observed. The larger blood vessels in the rabbit's conjunctiva and choroid showed a similar trend as the smaller blood vessel [Fig. 9(a)]. The larger blood vessels dilated slightly compared to the smaller vessels and started to constrict four minutes after the initial glycerol application. The larger blood vessels returned to baseline diameter at the end of the hydration cycle.

Table 2 summarizes the change in morphology and optical properties associated with the dehydration of the *in vivo* rabbit eye tissue upon glycerol application.

A QMRM with random effect was used for statistical analysis. We used 95% confidence interval ($p < 0.05$). In the QMRM,
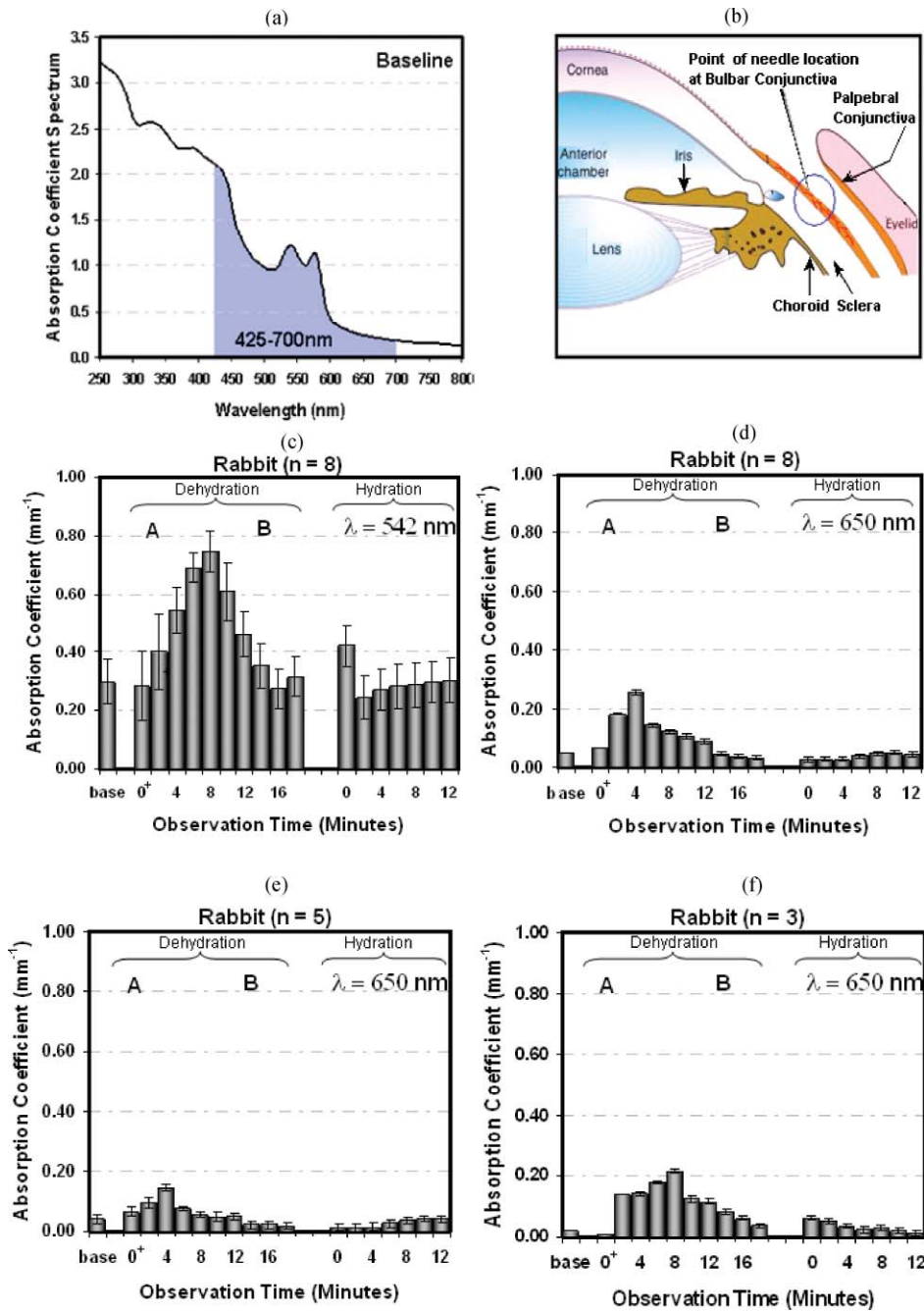
Fig. 7 Absorption spectrum of sclera collected (a) at baseline between 425 to 700 nm wavelength; (b) bulbar conjunctiva, the site of glycerol injection with superficial blood vessels; (c) calculated μ_a from all eight rabbits at 542 nm to capture strong blood absorption between 525 to 600 nm wavelengths; (d) calculated μ_a at 650 nm wavelength without any effect from blood absorption between 630 to 700 nm wavelength; μ_a is separated into two subgroups (e) AM (morning measurement, $n = 5$) and (f) PM (afternoon measurement, $n = 3$) based on time difference. Region A and B represent increase and decrease of optical clearing of sclera, respectively. All values are statistically significant ($p < 0.05$) for both cycles (quadratic mixed regression model). Error bars in terms of standard deviation are computed based on the average of μ_a.

all data from the rabbits were combined for the analysis. The μ_s' and μ_a were significant for both the dehydration and hydration cycles. The detected melanin concentration, blood volume fraction, O_2 saturation, and change in blood vessel diameter were significant for both dehydration and hydration cycles. In addition, the time and quadratic time in the QMRM were significant for μ_s', μ_a, melanin concentration, blood volume fraction, and change in blood vessels diameter. However, the O_2 saturation

did not have any significant effect of time as a linear function; but, the quadratic effect of time was significant.

4 Discussion

4.1 Questions Raised by the Study

Methods that reduce scleral water content can alter collagen spacing and size. Hyperosmotic agents such as 100% anhydrous
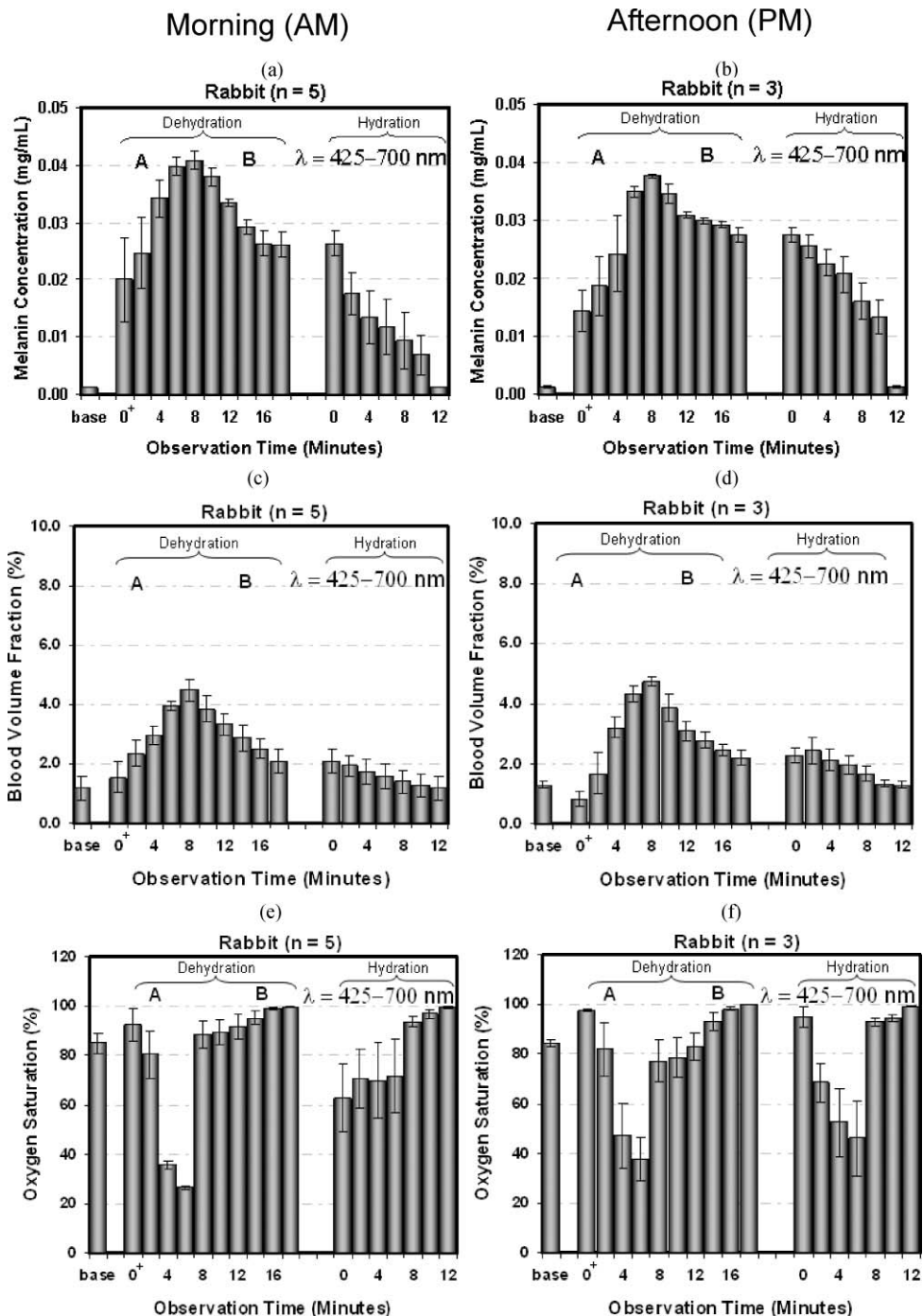
Fig. 8 Detected melanin concentration from rabbits conjunctiva and sclera (a) AM $n = 5$ (morning measurement, $n = 5$) and (b) PM (afternoon measurement, $n = 3$) during baseline indicates a trace amount of melanocyte that does not exist in the conjunctiva and sclera. This artifact was caused by setting the lower boundary of the inverse model to 0.001 mg/ml for smooth execution of the algorithm. Blood volume fraction of two subgroups of rabbits (c) and (d) conjunctiva and sclera at baseline; dehydration leads to optical clearing of sclera and increases visibility of choroidal layer leading to greater detection of blood volume fraction. Oxygen saturation of two subgroups of rabbits (e) and (f) conjunctiva and sclera at baseline; dehydration leads to acute inflammatory response causing blood vessel dilation, slower blood flow, and decreased O_2 saturation. The hydration cycle starts with the application of 0.9% saline that decreases optical clearing of eye. Region A and B represent an increase and decrease of optical clearing of sclera, respectively. Based on a quadratic mixed regression model, blood volume fraction and oxygen saturation are statistically significant ($p < 0.05$) for both dehydration and hydration cycles. However, the detection of melanin concentration is only significant for the hydration cycle. Error bars in terms of standard deviation are computed for all averaged optical properties.
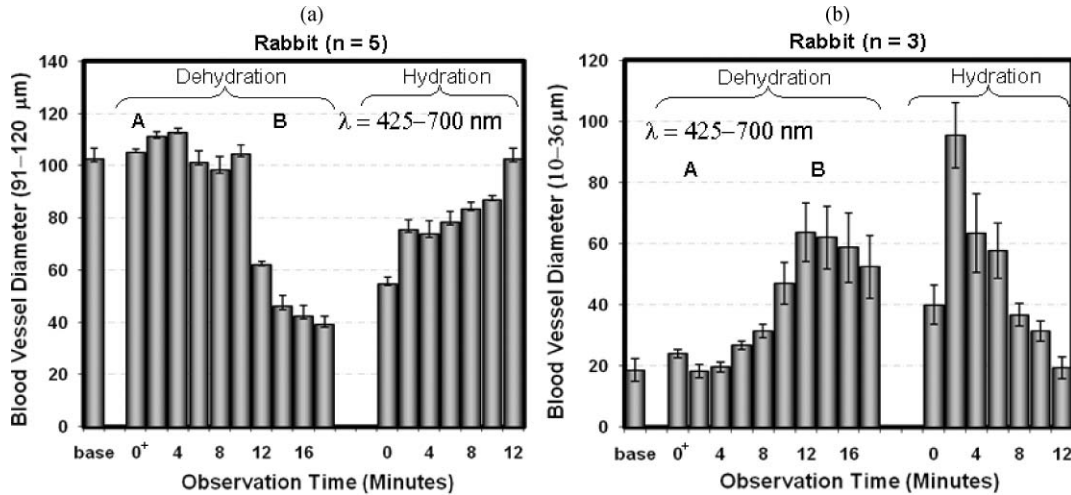
Fig. 9 Blood vessel diameter of rabbi t(a) ($n = 5$) with 91 to 120 μm and (b) ($n = 3$) with 10 to 36 μm in conjunctiva (sclera is mostly avascular) at baseline; during dehydration the injection of 100% anhydrous glycerol leads to acute inflammatory response causing smaller (10 to 36 μm) blood vessel to dilate and reduces blood volume fraction with decreased O_2 saturation; however, larger blood vessels (91 to 120 μm) dilate much slower than the smaller blood vessel, and followed by a gradual decrease in diameter and hydration with 0.9% saline, optical clearing of sclera decreases. Region A and B represent an increase and decrease of optical clearing of sclera, respectively. All values are statistically significant ($p < 0.05$) for both cycles (quadratic mixed regression model). Error bars in terms of standard deviation are computed based on the average of all blood vessels diameter.

glycerol can optically clear the sclera and have been shown to affect the local vascular system. We have studied the dynamics of the vascular system that comes in contact with glycerol during optical clearing. Some important questions remain. Is there a closure of blood vessels in the optically cleared eye tissue as reported when glycerol contacts *in vivo* rat and hamster dermis? Why is there a difference in blood vessel diameter between AM and PM measurements? These issues are discussed in the following paragraphs.

4.2 Optical Clearing Methods

Althoughthe same volume of glycerol was applied using two different optical clearing methods, direct application and injection, the rate of optical clearing of sclera greatly varied. The sclera quickly cleared (within 5 to 10 s) with the topical application of glycerol directly through an incision; whereas, for the injection method the clearing started after three minutes. Moreover, glyc-

erol applied with the direct application method spread over a larger area of the scleral surface than the injection method. Observation suggested that the injection method of glycerol held the volume of glycerol in a blister form in the sub Tenon's area (an extremely thin layer between the bulbar conjunctiva and sclera), which provides a diffusion barrier and restricted the spread of glycerol to areas surrounding the injection site.

4.3 Morphological Changes

Clearing the sclera with glycerol improves visualization of the *in vivo* choroid space. Rapid clearing of a circular pattern with 1.5 cm diameter optical window is achieved by making an incision in the conjunctiva and directly applying 0.1 ml of glycerol to the sclera. The reduction in light scattering is quantified using the injection method of glycerol application, which slowed the clearing process so DOS measurements could be made. Moreover, the injection method is less invasive compared to

Table 2 Time line for dehydration cycle only for injection method in eye tissue (AM only).

Time line	0+ min (30 s)	3 min	8 min	18 min
Morphology	No visible change to sclera	First sign of dehydration and a choroidal layer is visible	Maximum visibility of the choroidal layer (1.5 cm diameter) from the conjunctiva	Decreases visibility
Optical Properties				
1. Absorption (542 nm)	Slight increase in absorption	0.6 times increase	1.2 times increase	Similar to 0+ min
2. Reduced scattering coefficient	0.17 times decrease	0.32 times decrease	0.50 times decrease	Increase and similar to 0+ min

the incision method. According to several studies,[11,12,21] saline directly applied to the cleared sclera rapidly diffused through the sclera restoring the natural osmotic balance, returning the anterior sclera to its natural state within seconds. Although tissue restoration or reversal of the morphological change during the hydration cycle is rapid (five seconds), the time required for optical properties to reach the baseline measurement are relatively slow (12 min). Specifically, the detected melanin concentration gradually decreased as the water diffuses into the dehydrated sclera. However, 10 min after applying saline, water increased collagen spacing and size to the native level and the sclera became opaque. The nonlinear diffusion rate was noted and explained by Ghosn et al., where a (hyperosmotic agent) diffusion rate of glucose solution was measured in the *in vitro* rabbit eye.[36] The glucose diffusion rate was nonlinear across the sclera due to size, distribution, orientation, and packaging of collagen bundles of the three different scleral layers (episclera, stroma, and lamina fusca). This nonlinearity produced a much faster diffusion rate in stroma compared to the epithelium layer. Thus, it was possible to have a nonlinear diffusion rate of saline across the various layers of *in vivo* sclera. When we applied saline through the conjunctiva, the epithelium layer of sclera hydrated first followed by the stromal layer. The first eight minutes of the hydration process was comparatively slow and showed a linear decrease in detection of melanin concentration as the sclera starts to become opaque. However, when the saline reached the stromal layer, the diffusion rate increases and the entire tissue quickly hydrates. Thus, 10 to 12 min after hydrating the tissue, a sharp decrease was observed in the melanin concentration as the choroidal layer became completely invisible from the conjunctival surface.

4.4 *Diffuse Optical Spectroscopy Inverse and In Vivo Eye Models*

Light penetration depth increased as glycerol removed water from the sclera. We hypothesized that there are three different scenarios that govern the dynamic changes: 1. at baseline, sclera was highly scattered and collimated light penetrated a few micrometers through conjunctiva and anterior sclera; 2. during glycerol induced dehydration, the sclera optically cleared, the light penetration depth increased, and the collimated beam reached the choroidal layer where most of the light was absorbed due to the high concentration of melanin; and 3. as the sclera became less transparent as water returned to the sclera without any outside hydration, the light penetration depth decreased and scattering increased in the sclera (as illustrated in Figs. 6 and 7).

The DOS system provided a unique opportunity to compute optical properties and blood dynamics from the remitted spectrum during the application of a hyperosmotic agent. The technology developed for optical analysis of the multilayered skin is not that dissimilar to the eye. In this study, the LUT-based DOS inverse model estimated the value of the baseline *in vivo* optical properties as $\mu'_s = 2.8$ mm^{-1} at 630 nm, $\mu_a = 0.3$ mm^{-1} at 542 nm, and 0.005 mm^{-1} at 650 nm. These values were slightly lower than the physiological range of μ'_s(4.3 mm^{-1} at 630 nm) and μ_a (0.55 mm^{-1} at 542 nm and 0.4 mm^{-1} at 650 nm), respectively, for porcine *in vitro* sclera measured with an integrating sphere.[28] The main difference was the white sclera that quenched the source beam until glycerol induced clearing

became significant. The highest observed value of μ'_s in our study was 3.1 mm^{-1}, which was slightly lower than the *in vitro* value reported by Chan et al.[28] This difference may be due to higher absorption by chromophores such as red blood cell and melenocytes in *in vivo* tissue. O_2 absorption levels for *in vitro* and *in vivo* blood were also significantly different.

4.5 *Changes in Optical Properties*

The dynamic changes in DOS data attest to the diffusion time of the hyperosmotic agent through the sclera that is dependent upon the method of applying glycerol. The injection method reduces the volume of glycerol reaching the sclera relative to the direct method, which requires a small incision. Clearly, DOS results are initially governed by the highly scattering sclera and shift to the properties of the choroidal layer as the sclera becomes optically clear. Based on the changes in morphology and optical properties, the clearing of a 300-μm thick rabbit sclera takes approximately eight minutes using the injection method.

The accuracy of the absolute magnitude of computed optical properties was impacted by assumptions associated with the inverse problem. During experiments, the hyperosmotic agent caused a rapid increase in optical depth of the sclera as μ'_s decreased. The calibration phantoms had a constant thickness. In contrast, the physical thickness of the local sclera decreased as the clearing agent dehydrated the sclera.[36] Therefore, modification of the inverse algorithm is necessary for precise estimations of these dynamic optical properties with various tissue thicknesses.

Nevertheless, the results paint a remarkable picture of the dynamic changes taking place in the sclera and choroidal layers of the *in vivo* rabbit eye. The technique provides a tool for comparing the dynamic response of different agents and methods for delivery of the clearing agents upon optical properties.

The observed changes in optical properties in the sclera and choroidal layers are associated with the morphological changes induced by glycerol. Glycerol may trigger an inflammatory response owing to osmotic equilibrium deviations. In an acute inflammatory response, water leaves blood vessels and enters into the interstitial and sub-epithelial space (producing a blister), which may be masked by the glycerol at the injection site. Since penetration depth increases as μ'_s decreases, the DOS system is able to detect melanin and blood volume fraction from the highly vascular choroidal layer when the sclera is cleared.

4.5.1 *Blood dynamics*

The simple hypothesis that the glycerol would reduce blood volume fraction of the blood vessels of conjunctiva and choroid became complicated, considering the data from Figs. 8 and 9. First, there was the dichotomy in the computed diameter of blood vessels for AM and PM experiments (Fig. 9) and values of μ_a [Figs. 7(c) and 7(d)]. Small blood vessels diameters (PM, $n = 3$) were associated with afternoon experiments while larger diameters were identified during morning experiments (AM, $n = 5$).

In this study, we have shown that μ_a of rabbit's eye tissue is governed by the presence of blood and melnocytes. The intensity of μ_a varies slightly between the AM and PM subgroups. The slightly higher μ_a during the afternoon may be due to the dilation of the blood vessels, which causes an increase in

blood volume fraction as opposed to the morning measurements where blood vessel diameter decreased during the dehydration cycle. The blood volume fraction in the choroid is primarily modulated by the local tissue O_2 saturation and carbon dioxide (CO_2). Nitric oxide (NO) also regulates blood circulation during induction of hyperoxia in rabbits.[37] Vessel diameter and blood volume fraction along with wall shear rate transiently decreased during artificially induced hyperoxia with 100% O_2 saturation.[37] Previous studies revealed that endothelin (ET)-1, a protein, played a major role in hyperoxia-induced vasoconstriction via binding to ET type A receptor of smooth muscle in humans[38] and animals such as rabbits and newborn pigs.[39–41] There was a biphasic response to exogenous endothelin (ET)-1 on choroidal vessels of rabbit, suggesting that endogenous ET-1 preferentially elicits vasodilation via binding to ET type B receptor of vascular endothelium, most likely by stimulating endothelial NO release.[42]

During the afternoon measurements ($n = 3$) small blood vessels showed an increase in diameter when O_2 saturation reached a hyperoxia level or 99 to 100% saturation during the dehydration cycle. The presence of NO may stimulate dilation in the smaller blood vessels unlike morning measurements where larger blood vessels experience vasoconstriction. The difference in dilation patterns between the AM and PM subgroups based on the size of the blood vessels may be explained by Brubaker.[43] According to Brubaker, blood vessel diameter in the eye is not constant throughout the day due to the water dynamics. The aqueous humor production and filtration rate in ciliary body varies diurnally: it is normally 3.0 μl/min in the morning, 2.4 μl/min in the afternoon, and further drops to 1.5 μl/min at night. It is possible that during the morning hours the aqueous humor production masked the effect of NO on the choridal blood vessels and induced a decrease in blood vessel diameter. Therefore, it is hypothesized that a local transmitter such as NO regulates vessel diameter at the conjunctiva and choroidal layers of the rabbit's eye.

In our study, we have identified two different ranges of blood vessel diameters (91 to 120 μm and 10 to 36 μm) in rabbit eyes. These different ranges of blood vessels could be explained by Ninomiya et al. who has used a scanning electron microscopy to investigate the micro-vascular architecture of choroid and the anterior segment of the Yorkshire pig eye.[44] Capillaries at bulbar conjunctiva have a sparse capillary network with 16.0 μm diameters and a well-developed venous network ranging between 33.3 to 99.0 μm. Capillaries at choroid are flattened with a luminal diameter of 8.9 to 13.9 μm. Arteries and veins at the choroidal layer are 93 μm and 120 to 138 μm in diameter, respectively. The detected blood vessel diameters in our study between AM and PM subgroups are within these physiological ranges. Thus, it is possible that during the morning measurement we are able to identify more arteries and veins, respectively, from the bulbar conjunctiva and the choroidal layers due to rested eye unlike the afternoon measurement. In other words, the microvasculature found in our study illustrates a complex architecture of blood vessel diameters typical of the rabbit eye.

Although, we initially hypothesized that blood volume fraction in microvasculature of eye tissue decreased during the dehydration cycle, our study identified how different diameter blood vessels dynamically changed in diameter in the presence of glycerol. These changes in diameter could lead to an alteration in

blood volume fraction of these microvasculature. According to our study, smaller blood vessels in the PM subgroup dilated and led to an increase in blood volume fraction unlike larger blood vessels. During the morning measurements, the larger blood vessels may lead to vasoconstriction as the diameter reduced to one third of its original diameter after dehydrating the tissue. These differences in vessel diameter and their reduction in blood volume fraction in the presence of hyperosmotic agent may be a physiological phenomenon such as inflammation. Inflammation can cause vasodilation and an increase in blood volume inside the vessel. In our study, the larger blood vessels showed slight vasodilation followed by vasoconstriction during the dehydration cycle. It could be that the larger blood vessels are less affected by glycerol and lead to minor inflammation compared to smaller blood vessels.

4.5.2 O_2 saturation

O_2 saturation immediately increases after glycerol application at 0^+ min, followed by a nonlinear decrease as sclera dehydrates and reflectance spectra is obtained from the deeper layers. At the end of the dehydration and hydration cycles, O_2 saturation reached a hyperoxic level. The 99 to 100% saturation in O_2 level could be due to an acute inflammatory response where blood vessels are subjected to increased permeability and plasma exits into the extra vascular network.[45–47] In the native (pre-glycerol) blood vessels, the majority of blood cells are concentrated in the center of the stream, with an increased concentration of plasma near the walls.[45] This characteristic is important for keeping the viscosity near the walls at a minimum so that peripheral resistance is lower than it would be if the cells were uniformly distributed. When blood plasma escapes into the extra-vascular network, this property is lost and flow in the blood vessels is reduced and may influence the O_2 saturation because there is greater drag on the walls.[46]

Aside from simply inducing an osmotic imbalance that results in water loss, it is also possible that glycerol enters the lumen of the blood vessels by diffusion. The main issue of concern if 100% anhydrous glycerol enters the vessels is the osmotic shift in red blood cells. The application of glycerol to red blood cells leads to an initial shrinking of the cells as intracellular water leaves rapidly, followed by swelling when intracellular water reenters the cells; glycerol continues to enter the cells by facilitated diffusion.[45] This phenomenon ultimately leads to an increase in O_2 saturation, which was observed in this study.

5   Conclusion

This study verified an improved visualization of the choroidal layer by creating an optical window through the sclera induced by 100% anhydrous glycerol. Morphological changes were observed in different rates after two different methods of glycerol application to the rabbit eye. Rapid clearing was achieved through the incision method, unlike the injection method. The DOS system with the LUT algorithm provided a method to address the changes in optical properties associated with the alteration of physical properties upon the application of a hyperosmotic agent. We had not anticipated significant differences in change pattern in optical properties during morning and afternoon measurements. Although, this aspect may contribute to the

complexity of analyzing the process, the study promises a novel way of optically accessing deep layers of the eye for treating ocular diseases without any invasive surgery.

References

1. V. V. Bakutkin, I. L. Maksimova, T. N. Semyonova, V. V. Tuchin, and I. L. Kon, "Controlling of optical properties of sclera," *Proc. SPIE* **2393**, 137–141 (1995).
2. V. V. Tuchin, I. L. Maksimova, D. A. Zimnyahkov, I. L. Kon, A. K. Mavlutov, and A. A. Mishin, "Light propagation in tissues with controlled optical properties," *Proc. SPIE* **2925**, 118–142 (1996).
3. V. V. Tuchin, I. L. Maksimova, D. A. Zimnyakov, I. L. Kon, A. K. Mavlutov, and A. A. Mishin, "Light propagation in tissues with controlled optical properties," *J. Biomed. Opt.* **2**, 401–417 (1997).
4. V. V. Tuchin, *Optical Clearing of Tissues and Blood*, Monograph Vol. PM 154, Chapt. 2, pp. 23–58 and subsection 8.3, pp. 188–191, SPIE Press, Bellingham, WA (2006).
5. A. N. Bashkatov, V. V. Tuchin, E. A. Genina, Y. P. Sinichkin, N. A. Lakodina, and V. I. Kochubey, "The human sclera dynamic spectra: in vitro and in vivo measurements," *Proc. SPIE* **3591**, 311–319 (1999).
6. V. V. Tuchin, J. Culver, C. Cheung, S. A. Tatarkova, M. A. DellaVecchia, D. Zimnyakov, A. Chaussky, A. G. Yodh, and B. Chance, "Refractive index matching of tissue components as a new technology for correlation and diffusing-photon spectroscopy and imaging," *Proc. SPIE* **3598**, 111–120 (1999).
7. V. V. Tuchin, "Coherent soptical techniques for the analysis of tissue structure and dynamics," *J. Biomed. Opt.* **4**(1), 106–124 (1999).
8. Z. S. Sacks, R. M. Kurtz, T. Juhasz, and G. A. Mourau, "High precision subsurface photodisruption in human sclera," *J. Biomed. Opt.* **7**(3), 442–450 (2002).
9. E. A. Genina, A. N. Bashkatov, Yu. P. Sinichkin, and V. V. Tuchin, "Optical clearing of the eye sclera in vivo caused by glucose," *Quantum Electron.* **36**(12), 1119–1124 (2006).
10. M. G. Ghosn, E. F. Carbajal, N. Befrui, V. V. Tuchin, and K. V. Larin, "Differential permeability rate and percent clearing of glucose in different regions in rabbit sclera," *J. Biomed. Opt.* **13**, 021110 (2008).
11. G. Vargas, E. K. Chan, J. K. Barton, H. G. Rylander III, and A. J. Welch, "Use of an agent to reduce scattering in skin," *Lasers Surg. Med.* **24**, 133–141 (1999).
12. G. Vargas, K. F. Chan, S. L. Thomsen, and A. J. Welch, "Use of osmotically active agents to alter optical properties of tissue: effects on the detected fluorescence signal measured through skin," *Lasers Surg. Med.* **29**, 213–220 (2001).
13. G. Vargas, "Reduction of light scattering in biological tissue: implications for optical diagnostics and therapeutics," Doctoral Dissertation, The University of Texas at Austin (2001).
14. K. P. Boergen, R. Birngruber, V. P. Gabel, and F. Hillenkamp, "Experimental studies on controlled closure of small vessels by laser irradiation," *Lasers Surg. Med. Biol. Proc. Berlin* **5**, 15.1–15.9 (1977).
15. R. T. Zaman, A. B. Parthasarathy, G. Vargas, B. Chen, A. K. Dunn, H. G. Rylander III, and A. J. Welch, "Perfusion in hamster skin treated with glycerol," *Lasers Surg. Med.* **41**, 492–503 (2009).
16. N. Rajaram, T. H. Nguyen, and J. W. Tunnell, "Lookup table-based inverse model for determining optical properties of turbid media," *J. Biomed. Opt.* **13**(5), 050501 (2008).
17. J. R. Mourant, T. Fuselier, J. Boyer, T. M. Johnson, and I. J. Bigio, "Predictions and measurements of scattering and absorption over broad wavelength ranges in tissue phantoms," *Appl. Opt.* **36**(4), 949–957 (1997).
18. J. C. Finlay and T. H. Foster, "Effect of pigment packaging on diffuse reflectance spectroscopy of samples containing red blood cells," *Opt. Lett.* **29**(9), 965–967 (2004).
19. R. L. van Veen, W. Verkruysse and H. J. Sterenborg, "Diffuse-reflectance spectroscopy from 500 to 1060 nm by correction for inhomogeneously distributed absorbers," *Opt. Lett.* **27**(4), 246–248 (2002).
20. L. Svaasand, E. Fiskerstrand, G. Kopstad, L. Norvang, E. Svaasand, J. Nelson, and M. Berns, "Therapeutic response during pulsed laser treatment of port-wine stains: dependence on vessel diameter and depth in dermis," *Lasers Med. Sci.* **10**(4), 235–243 (1995).
21. G. Vargas, A. Readinger, S. S. Dozier and A. J. Welch, "Morphological changes in blood vessels produced by hyper osmotic agents and measured by optical coherence tomography," *Photochem. Photobiol.* **77**(5), 541–549 (2003).
22. R. W. Stephenson, *Anatomy, Physiology and Optics of the Eye: A Textbook for Orthoptic Students*, Kimpton Publishers, London (1973).
23. S. C. Nemeth, *Ocular Anatomy and Physiology*, Slack Inc. Publishers, Thorofare, NJ (2007).
24. Y. Feng and T. L. Simpson, "Corneal, limbal, and conjunctival epithelial thickness from optical coherence tomography," *Optom. Vision Sci.* **85**(9), 880–883 (2008).
25. S. S. Hayreh, "Segmental nature of the choroidal vasculature," *Br. J. Ophthalmol.* **59**(11), 631–648 (1975).
26. A. R. Young, "Chromophores in human skin," *Phys. Med. Biol.* **42**, 789–802 (1997).
27. R. T. Zaman, P. Diagaradjane, J. C. Wang, J. Swartz, N. Rajaram, K. L. Gill-Sharp, S. H. Cho, H. G. Rylander, D. J. Payne, S. Krishnan, and J. W. Tunnell, "*In vivo* detection of gold nanoshells in tumors using diffuse optical spectroscopy," *IEEE J. Sel. Top. Quantum Electron.* **13**(6), 1715–1720 (2007).
28. E. K. Chan, B. Sorg, D. Protsenko, M. O'Neil, M. Motamedi, and A. J. Welch, "Effects on compression on soft tissue optical properties," *IEEE J. Sel. Top. Quantum Electron.* **2**(4), 943–950 (1996).
29. T. J. Farrell, M. S. Patterson, and B. Wilson, "A diffusion theory model of spatially resolved, steady-state diffuse reflectance for the noninvasive determination of tissue optical properties *in vivo*," *Med. Phys.* **19**, 879–888 (1992).
30. A. Kienle and M. S. Patterson, "Improved solutions of the steady-state and the time-resolved diffusion equations for reflectance from a semi-infinite turbid medium," *J. Opt. Soc. Am. A* **14**, 246–254 (1997).
31. N. Rajaram, A. Gopal, X. J. Zhang, and J. W. Tunnell, "Experimental validation of the effects of microvasculature pigment packaging on *in vivo* diffuse reflectance spectroscopy," *Lasers Surg. Med.* **42**(7), 680–688 (2010).
32. A. J. Welch and M. J. Gemert, *Optical-Thermal Response of Laser-Irradiated Tissue*, Appendix to Chapt. 8, Plenum, New York (1995).
33. S. Prahl, "Tabulated molar extinction coefficient for hemoglobin in water," http://omlc.ogi.edu/spectra/hemoglobin/index.html, accessed 7/24/09.
34. B. T. West, K. B. Welch, and A. T. Galecki, *Linear Mixed Models: A Practical Guide Using Statistical Software*, Chapman and Hall, London (2007).
35. C. R. Ethier, M. Johnson, and J. Ruberti, "Ocular biomechanics and biotransport," *Annu. Rev. Biomed. Eng.* **6**, 249–273 (2004).
36. M. G. Ghosn, V. V. Tuchin, and K. V. Larin, "Depth-resolved monitoring of glucose diffusion in tissues by using optical coherence tomography," *Opt. Lett.* **31**(15), 2314–2316 (2006).
37. J. W. Kiel, "Endothelin modulation of choroidal blood flow in the rabbit," *Exp. Eye Res.* **71**, 543–550 (2000).
38. S. Dallinger, G. T. Dorner, R. Wenzel, U. Graselli, O. Findl, H. G. Eichler, M. Wolzt, and L. Schmetterer, "Endothelin-1 contributes to hyperoxia-induced vasoconstriction in the human retina," *Invest. Ophthalmol. Visual Sci.* **41**, 864–869 (2000).
39. Y. Zhu, T. S. Park, and J. M. Gidday, "Mechanisms of hyperoxia-induced reductions in retinal blood flow in newborn pig," *Exp. Eye Res.* **67**, 357–369 (1998).
40. C. Takagi, G. L. King, H. Takagi, Y. W. Lin, A. C. Clermont, and S. E. Bursell, "Endothelin-1 action via endothelin receptors is a primary mechanism modulating retinal circulatory response to hyperoxia," *Invest. Ophthalmol. Visual Sci.* **37**(10), 2099–2109 (1996).

41. K. Nishimura, C. E. Riva, S. Harino, P. Reinach, S. D. Cranstoun, and S. Mita, "Effects of endothelin-1 on optic nerve head blood flow in cats," *J. Ocul. Pharmacol. Ther.* **12**, 75–83 (1996).

42. J. W. Kiel, "Endothelin modulation of choroidal blood flow in the rabbit," *Exp. Eye Res.* **71**, 543–550 (2000).

43. R. F. Brubaker, "Measurement of aqueous flow by fluorophotometry," *The Glaucomas*, pp. 337–344, Mosby, St. Louis (1989).

44. H. Ninomiya and T. Inomata, "Mirovascular anatomy of the pig eye: scanning electron microscopy of vascular corrosion casts," *J. Vet. Med. Sci.* **68**(11), 1149–1154 (2006).

45. W. Verkruyssa, M. Khan, B. Choi, L. O. Svaasand, and S. J. Nelson, "Measuring the effects of topically applied skin optical clearing agents and modeling the effects and consequences for laser therapies," *Proc. SPIE* **5695**, 278–287 (2005).

46. J. B. Walter and M. S. Israel, *The Inflammatory Reaction In General Pathology*, Chapt. 6, Churchill Livingston, London (1974).

47. L. M. Wahl and S. M. Wahl, *Inflammation in Wound Healing. Biochemical and Clinical Aspects*, pp. 40–53, Saunders, Philadelphia (1992).